Journal of
Materials Chemistry A

Accepted Manuscript

This is an *Accepted Manuscript*, which has been through the RSC Publishing peer review process and has been accepted for publication.

Accepted Manuscripts are published online shortly after acceptance, which is prior to technical editing, formatting and proof reading. This free service from RSC Publishing allows authors to make their results available to the community, in citable form, before publication of the edited article. This *Accepted Manuscript* will be replaced by the edited and formatted *Advance Article* as soon as this is available.

To cite this manuscript please use its permanent Digital Object Identifier (DOI®), which is identical for all formats of publication.

More information about *Accepted Manuscripts* can be found in the **Information for Authors**.

Please note that technical editing may introduce minor changes to the text and/or graphics contained in the manuscript submitted by the author(s) which may alter content, and that the standard **Terms & Conditions** and the **ethical guidelines** that apply to the journal are still applicable. In no event shall the RSC be held responsible for any errors or omissions in these *Accepted Manuscript* manuscripts or any consequences arising from the use of any information contained in them.

Journal of
Materials Chemistry A

RSCPublishing

ARTICLE

A Novel Complementary Absorbing Donor-Aceptor Pair in Block Copolymers Based on Single Materials Organic Photovoltaics

Cite this: DOI: 10.1039/xoxxoooooo

Received xxxxxxxxxxxx,
Accepted xxxxxxxxxxxx

DOI: 10.1039/xoxxoooooo

www.rsc.org/

Sermet Koyuncu,[a]* Hsin-Wei Wang,[b] Feng Liu,[b] Kamil Bugra Toga,[b] Weiyin Gu,[b] and Thomas P. Russell[b]*

We report on first synthesis of highly crystalline donor acceptor low band gap block copolymer by using diketopyrollopyrolle (DPP) as low band gap block and perylenebisimide (PDI) as strong acceptor block. All important prerequisites for PV application such as strong and broad optical absorption, compatible HOMO-LUMO levels can be accomplished and combined on the one macromolecule at the same time. Besides, microphase separation is achieved by solvent annealing the film in dichloromethane and the PV performance is improved from 0.25% to 0.89%. The morphology and performance of this single component system can be enhanced by further improvements in the processing conditions.

Introduction

The discovery of conducting polymers has promoted a global effort in commercialization of organic semiconductors that offer unique advantages over traditional systems as a result of their light weight, low cost, multi-optional synthetic strategies, solution processability, and ease of fabrication.[1-3] The design and development of new polymeric materials as active components in organic solar cells and organic light emitting diodes have increased the motivation of academia and industry to substitute inorganic materials with the organic ones in optoelectronic systems. In organic photovoltaic (OPV) devices, the essential parameters such as control of morphology and π conjugation can be determined by tuning processing conditions for efficient device performance.[4-9] Proper film-formation must be combined with suitable chemical structure to fulfill the requirements of light absorption, charge separation, and charge transport in confined geometries.[10, 11] The ability to control the self-assembly of nano-structured materials is key in developing optimized devices. Morphological control at the nanoscale is required to enhance the interaction between the components and to ensure long-term device stability. Block copolymers present one strategy to meet these requirements, since they microphase separate into nanoscopic spherical, cylindrical, gyroid, or lamellar morphologies,[12] opening the possibility of controlling the type, size, and orientation of the domains. Thelakkat and co-workers,[13] studied diblock copolymers containing a poly(4-vinyl triphenylamine) (electron donor) block and a perylenebisimide acrylate (electron acceptor) block. The reported maximum power conversion efficiencies in devices constructed from these diblock copolymers was only 0.35%. Thelakkat *et al.* and Russell *et al.* investigated the size effects in OPV materials from molecular scale through mesoscopic to macroscopic scale using the principles of self-assembly of block copolymers.[14-16] In both studies, a polymerizable perylenebisimide derivative (acceptor) was packed into crystalline microdomains in a polythiophene matrix (donor), as a result of strong π-π stacking between adjacent perylenebisimide moieties.[14, 15] Despite achieving microphase separation, power conversion efficiencies of the devices constructed from these copolymers were only 0.49%.[15]

For almost two decades, research on intrinsically-conductive organic materials has demonstrated that the efficient power conversion relies on the control of the band gap of extended π-conjugated systems.[17-20] Active materials for electronic and photonic applications must present appropriate absorption and/or emission properties, since highest occupied and lowest unoccupied molecular orbital (HOMO and LUMO) energy levels have a strong effect on charge-transport properties. Other key attributes of the hole-conducting polymer essentially for optimal performance include a broader absorption of light, a relatively low HOMO level, and a higher hole mobility. There are three useful strategies to satisfy these requirements: *i)* low band gap approach via donor-acceptor combination for a narrower E_g and deeper LUMO level; *ii)* addition of electron-withdrawing groups to depress the HOMO level; and *iii)* maintaining two-dimensional conjugation for broad absorption and higher hole mobility.[21, 22] Better planarity of main chain and reduction in steric hindrance of side chains can be considered for a stronger π-π stacking and increased in hole mobility.[23] Furthermore, the molecular weight of the polymers also influences the OPV performance, emerging an optimal molecular weight in most cases.[24] To produce high efficiency OPV devices, researchers should attempt to increase molecular weight while maintaining a better solubility. Recently, ~10% efficiency has been obtained by using these approaches.[25-32]

Herein, we report the synthesis of a highly crystalline donor acceptor low band gap copolymer consisting of diketopyrollopyrolle (DPP) as the donor and perylenebisimide (PDI) as the acceptor component. In order to obtain the desired donor acceptor low band gap polymers with broad absorption, DPP based macroinitator (absorbance in blue and red regime) was linked to electron accepting PDI molecules (absorbance in green regime). Such material offers a strong and broad optical absorption of the visible spectrum; compatible HOMO-LUMO levels; and crystallinity driven phase separation. As a result, we have achieved 0.89% efficiency, which is one of the highest efficiency reported for single component solar cells.[33-35]

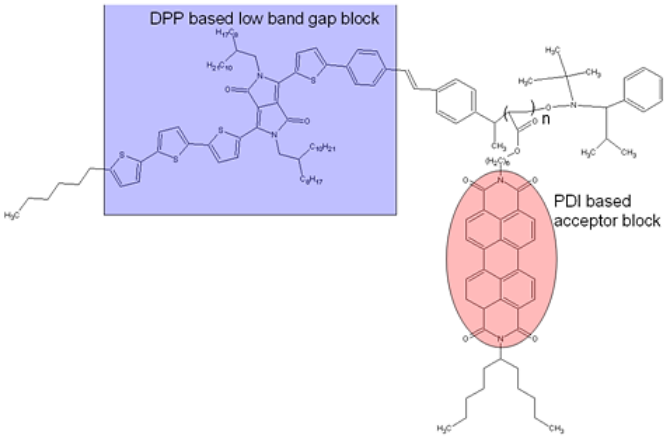

Fig. 1 Structure of DPP-PDI block copolymer

Results and discussion

The DPP based macroinitator was prepared in seven steps, and PDI based acrylic monomer in four steps. The DPP based macroinitator was used for polymerization of acryloyl based perylenebisimide monomer (see supporting information). ^{1}H-NMR data were used for the characterization of all molecules. The degree of polymerization (DP) was calculated in reference to the perylenebisimide block protons and selected DPP protons using ^{1}H-NMR of the block copolymer (Fig. S5†) and found 3-4. On the other hand, according to GPC data, M_w and PDI were found 7200 gmol^{-1} and 1.16, respectively, using a polystyrene standard ((Fig. S6†). The molecular weight measured by GPC is higher than that of calculated from ^{1}H-NMR, due to the rigid nature of DPP-PDI block copolymer.

Optical and electrochemical characterization of DPP-PDI block copolymers were carried out via UV-Vis absorption, photoluminescence (PL) and cyclic voltammetry (CV). The HOMO-LUMO band gaps were calculated using the same techniques. UV-Vis spectrum of the PDI-acceptor moiety in DCM solutions exhibits three characteristic absorption bands at λ_{max} = 459, 488 and 522 nm.[36] The DPP based macroinitator has two major absorption bands at λ_{max} ~ 375 and ~ 590 nm [37] which are attributed to the π–π* and intra-molecular charge transfer (ICT) bands, respectively (Fig. S7†). These bands in the copolymer do not show a dramatic shift in structure and in their intensity. A red shift was observed in the thin film due to π–π interaction in the solid state (Fig. S8†). Overall, the optical analyses show that the DPP-macroinitator and PDI-acceptor have complementary absorption properties in the visible and near IR regime. Owing to this property, a black polymer with broad absorption characteristics has been obtained (Fig. 2).

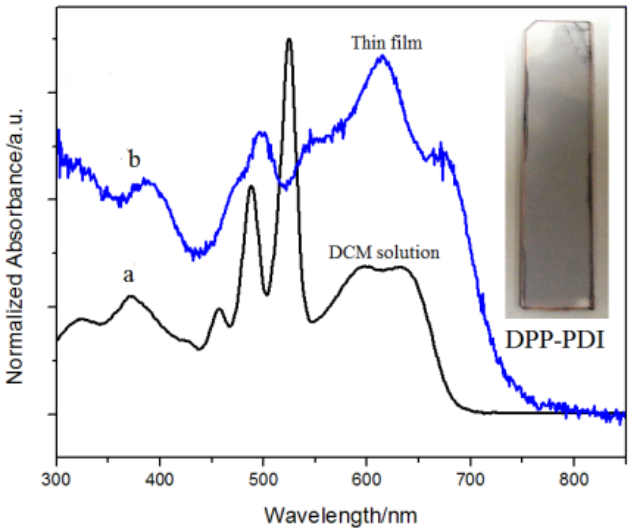

Fig. 2 Absorption spectra of DPP-PDI block copolymer a) in DCM solution b) on thin film

The photoluminescence PL behavior was characterized under similar conditions (0.02 mg mL^{-1} in DCM and/or in thin films). Fig. 3 shows a comparison of the PL spectra of the monomer, macroinitator and the DPP-PDI block copolymer. PDI-monomer exhibits strong emission bands at λ_{max} = 536, 562 and 625 nm (λ_{ex} = 488 nm).[36] The excitation of DPP-macroinitator at its absorption maxima (λ_{ex} = 380 nm) resulted in three distinct emission bands at 412, 445 and 775 nm. A large decrease in PL occurs upon polymerization of macromonomer in which DPP-macroinitator is covalently linked to the perylene-acceptor (λ_{ex} = 355 nm) (Fig S9†). The strong PL observed in thin films of the monomer and the macroinitiator was not seen in the thin films of the copolymer. Quenched PL in the copolymer can be explained by photo-induced electron transfer from the DPP (the low band gap block) to the PDI (the acceptor block) at the excited state (Fig 3).

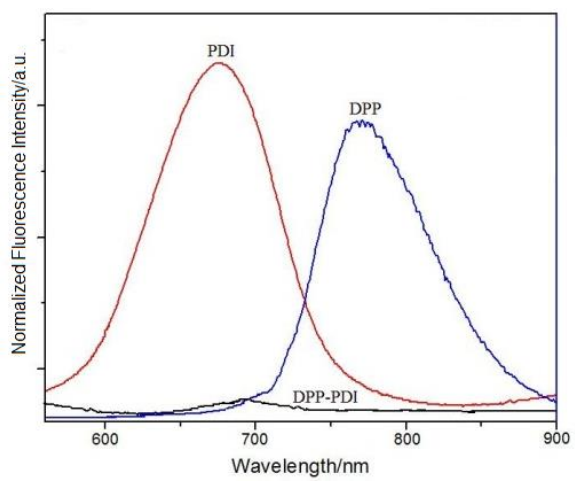

Fig. 3 Photoluminescence spectra of initial compounds and DPP-PDI block copolymer on thin film.

HOMO and LUMO energy levels and band gap, E_g of the DPP-PDI block copolymer can be calculated by using CV. In the cathodic scan regime, PDI-monomer exhibits characteristic reversible reduction from -0.40 to -0.46V ($E^{red1}_{PDI,1/2}$ = -0.43V), and -0.56 to -0.62V

($E^{red2}_{PDI,1/2}$ = -0.59V) which reflects the first and second one-electron stepwise reduction process of perylenebisimides. Furthermore, a reversible reduction of DPP was observed with a half wave potential at $E^{red1}_{DPP,1/2}$ = -1.06V. In the anodic regime, DPP showed two reversible oxidation peaks at 0.62 - 0.78V ($E^{ox1}_{DPP,1/2}$ = 0.70V) and 1.12–1.36V ($E^{ox2}_{DPP,1/2}$ = 1.24V) (Fig. 4). Finally, in the CV of DPP-PDI block copolymer, both the DPP oxidation-reduction and PDI reduction were clearly observed. These results indicate that there is no interaction between the DPP based low band gap macroinitator and PDI-acceptor in the neutral state.

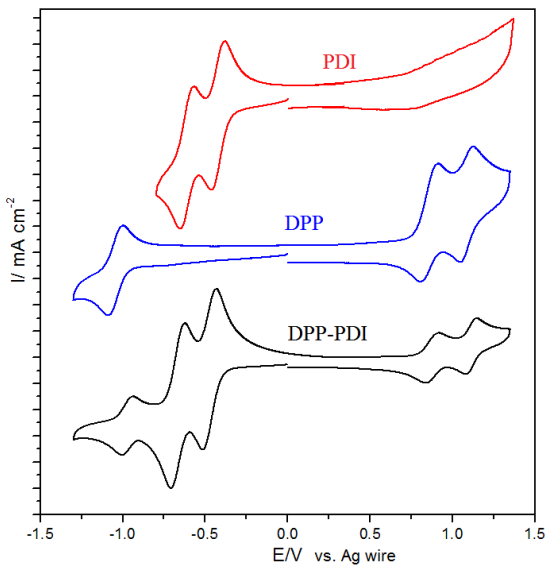

Fig. 4 CV curves of initial compounds and DPP-PDI block copolymer, $E°$(Fc/Fc+) = +0.41 V (vs. Ag wire)

Optical and electrochemical band gap results are summarized in **Table 1**. The band gap values are not identical, since significant fluorescence quenching was observed in the copolymer, although PDI monomer and DPP-macroinitator showed their distinct photoluminescence peaks. These results show that possible photo-induced electron transfer occurs from DPP as the low band gap block to PDI as the acceptor block in the excited state. Therefore, this new material holds promise as a good candidate for an efficient OPV device.

Table 1. Optical and electrochemical data of DPP-PDI block copolymer

Molecule	HOMO	LUMO	E_g[a]	E_g'[b]
PDI-monomer	-5.92[c]	-4.03	-	1.83
DPP-macroinitator	-5.15	-3.47	1.68	1.65
DPP-PDI block copolymer	-5.17	-4.08	1.09	1.65

[a] Electrochemical band gap [b] Optical band gap [c] Calculated by the subtraction of the optical band gap to the LUMO level; $E°$(Fc/Fc+) = +0.41 V (vs. Ag wire)

The thermal properties of the DPP-PDI copolymers were investigated by differential scanning calorimetry (DSC) (Fig 5). The solvent treated, desiccated raw material was initially heated above the melting temperature of the component blocks. The DSC trace of DPP-PDI has two peaks at 96.0 and 109.5 °C, corresponding to the melting temperatures of the blocks, respectively.[14] This reflects the easy crystallization of the blocks in solution. A single exotherm at 54.7 °C was observed when the block copolymer was slowly cooled from the melt, suggesting a co-crystallization of the DPP and PDI from the melt which limits the segregation of the components.

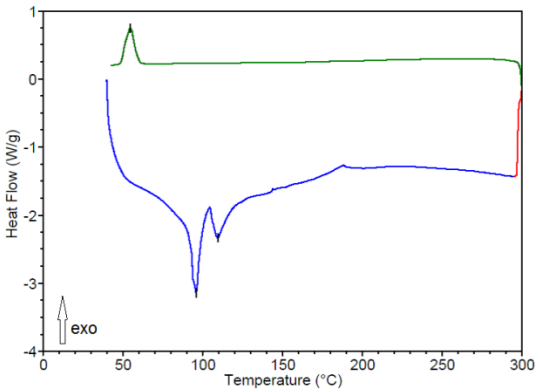

Fig. 5 DSC curve of DPP-PDI block copolymer

Solvent processing of DPP-PDI potentially leads to large grain sizes and high crystallinity. To maximize device efficiency, processing conditions need to be identified in order to control the size of the crystals. Films of copolymer were prepared by spin coating from chloroform (CF) and chlorobenzene (CB). The topography and phase contrast can be attributed to the crystalline domains of the PDI and DPP blocks (Fig. S10 and S11†). By thermal annealing at the melting point of each block (100 °C), the size of crystalline domains increases and grain growth proceeds without changing the orientation of the grains. However, this does not increase the charge separation between DPP and PDI phases. Lower device efficiency was found upon thermal annealing done in accordance with the DSC results.

To understand the role of morphology, photovoltaic devices based on the DPP-PDI copolymers were fabricated with the device structure of ITO/PEDOT:PSS (40 nm)/DPP-PDI (from 70 to 120 nm)/LiF (1 nm)/Al (100 nm). The device performance was measured at ambient conditions with an AM 1.5 solar simulator at 100 mW cm^{-2}. The device obtained by CB spin coating showed a better performance, considering AFM and TEM results where a finer crystalline texture was observed. Film thickness also played an important role in defining the morphology. The thinner films achieved by varying the spin speed or solution concentration yielded a finer crystalline texture. There was only a weak phase contrast evident by AFM, However, the small refinement in crystal texture (Fig.6a) enhanced the PV performance from 0.25% to 0.47%. By solvent annealing the film in DCM, further microphase separation was achieved (Fig.6b), and the PV performance was improved from 0.47% to 0.89% (Fig.7).

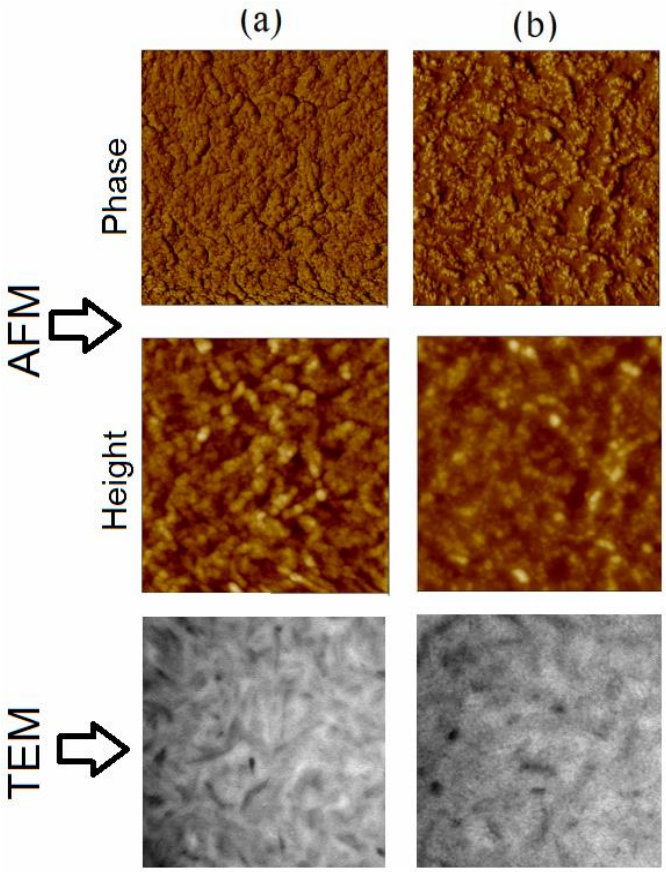

Fig. 6. AFM and TEM images of the DPP-PDI block copolymer thin film (from a 1 wt % CB solution at 2000 rpm) a) pristine film b) after annealing for 15 min in DCM vapor (each scale 3μm x 3μm)

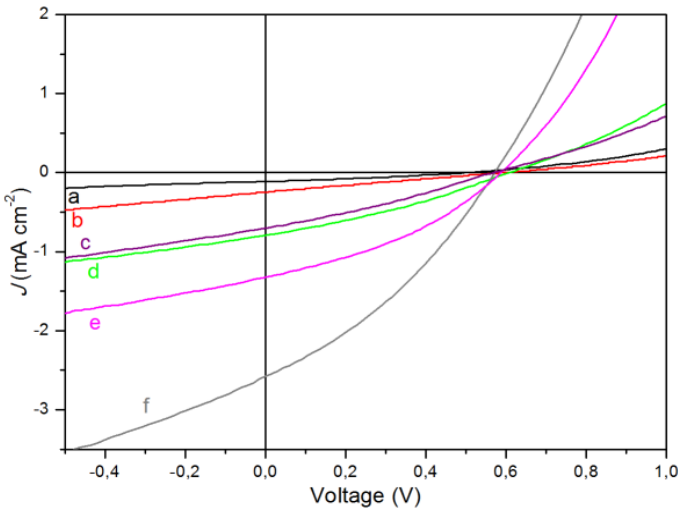

Fig. 7 J-V characteristics (AM 15G, 100mW cm^{-2}) of DPP-PDI block copolymer based devices (a) 120 nm-CF-annealing at 100 °C;(b) 120 nm-CB-annealing at 100 °C;(c)110 nm-CF; (d) 120 nm-CB; (e) 70 nm-CB; (f) 70 nm-CB-annealed by DCM for 15 min.

Table 2 Performance of ITO PEDOT:PSS/DPP-block-PDI/LiF-Al Bulk Heterojuction Photovoltaic Devices under a Simulated Photovoltaic Light with 100 mW cm^2 Illumination (AM 15G)

Sample code	Voc (V)	Jsc (mA/cm^2)	Fill Factor (%)	Efficiency (%)
1[a]	0.50	0.19	31.27	0.03
2[b]	0.59	0.41	24.15	0.06
3[c]	0.57	1.17	29.54	0.19
4[d]	0.61	1.32	31.12	0.25
5[e]	0.59	2.20	36.14	0.47
6[f]	0.57	4.30	33.60	0.89

[a]120 nm-CF-annealing at 100 °C; [b] 120 nm-CB-annealing at 100 °C; [c] 110 nm-CF; [d] 120 nm-CB; [e] 70 nm-CB; [f] 70 nm-CB-annealed by DCM for 15 min

On the other hand, the incident monochromatic photon-to-current conversion efficiency (IPCE) was measured at 600 nm leading to 45% of current (Fig. 8). A remarkable broad photocurrent response is obtained because of the complementary absorbance property of the DPP and PDI.

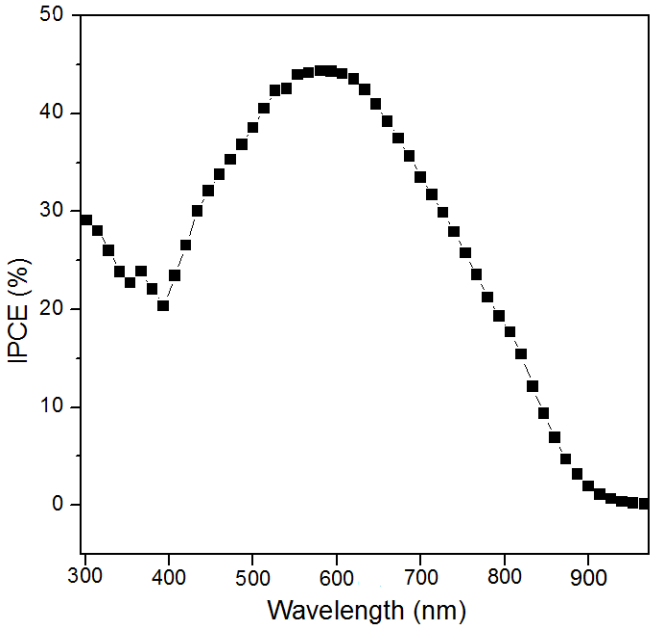

Fig.8. IPCE curve of DPP-PDI block copolymer based device

Conclusion

In summary, a novel block copolymer was synthesized based on a diketopyrollopyrolle (DPP) low band gap macroinitator and a perylenebisimide acceptor. Optical and electrochemical results show that the HOMO-LUMO levels and broad absorption properties of the DPP-PDI block copolymer are advantageous for photovoltaic device applications. The new copolymer also exhibits a broad absorption in the visible and near IR regime. Two exotermic peaks observed in DSC are strong indicators of the high crystallinity and phase separation. Larger crystalline domains resulted upon thermal annealing did not improve charge separation between the components and thus, displayed a lower performance. Finer crystal textures were achieved by reducing the film thickness, i.e. changing the processing conditions increased the efficiency from 0.25% to 0.89%. Further improvements in the processing conditions can clearly offer better morphology and, therefore enhance performance of this single component system.

Experimental Section

All synthetic steps were given in the supporting information. ^{1}H NMR (Bruker Avance DPX-400) spectra were recorded at 25 °C in deuterated chloroform ($CHCl_3$-d) and TMS as internal standard. Gel permeation chromatography (GPC) was measured in THF relative to polystyrene standards (Scientific Polymer Products) on a system equipped with a three-column set (Polymer Laboratories 300 x 7.5 mm; 5 μm; pore sizes, 10–5, 10–4, and 10–3 Å) and a refractive-index detector (HP 1047 A) at room temperature with a flow rate of 1 mL min^{-1}. Cyclic voltammetry (CV) technique used for electrochemical measurements was performed using BASi EC epsilon potentiostat-galvanostat system. The electrochemical cell includes an Ag wire as reference electrode (RE), Pt wire as counter electrode (CE) and platinium disk (0.02 cm^2) as working electrode (WE) immersed in 0.1 M $TBAPF_6$/DCM as the supporting electrolyte. CV measurements were carried under argon atmosphere. HOMO and LUMO energy levels of polymer were calculated according to the inner reference ferrocene redox couple $E°$(Fc/Fc+) = +0.41 V (vs. Ag wire) in DCM by using the formula $E_{HOMO} = -e(E_{ox} - E_{Fc}) + (-4.8\ eV)$ and $E_{LUMO} = -e(E_{red} - E_{Fc}) + (-4.8\ eV)$.[38] The electrochemical HOMO–LUMO energy levels were calculated from their oxidation and reduction onset values. UV-Vis spectra were recorded by Shimatszu UV3600 spectrophotometer. The absorption spectra of monomer and polymer were recorded in DCM solution and/or on transparent glass surface. The optical band gap (E_g) of products were calculated from their solid state low energy absorption edges ($E_g = 1241/\lambda_{onset}$).[18] Photoluminescence spectra were recorded on a PTIQM30 fluorescence spectrophotometer. Atomic Force Microscopy (AFM) images were obtained in both the height and phase-contrast mode using a Digital Instruments Dimension 3000 scanning force microscope in the tapping mode. Transmission electron microscopy (TEM) was performed using a JEOL 2000CX instrument at 200 kV accelerating voltage. DSC measurements were performed on a TA Q100 thermal analyzer at scanning rate of 10 °C min^{-1}.

Photovoltaic devices were fabricated on indium tin oxide (ITO) covered glass substrates with the structure of ITO/PEDOT:PSS (40 nm)/DPP-PDI (from 70 to 120 nm)/LiF (1 nm)/Al (100 nm). First, ITO electrodes were cleaned with detergent, deionized water, aceton and isopropanol and then oven-dried at 100 °C for 5h (please double check the drying time), and finally treated with oxygen plasma. Device production and current/voltage property measurements were conducted in a nitrogen filled glove box system (MBraun) (moisture <0.1 ppm; oxygen <0.1 ppm). An approximately 40 nm thick layer of poly(3,4-ethylenedioxythiophene) doped with poly(styrenesulfonate) (PEDOT: PSS) was spin-coated from aqueous solution (Baytron PH500, HC Stack Inc). The substrate was dried for 10 min. at 150 °C. On top of the PEDOT:PSS, the active layer (from 70 to 120 nm) was spin-coated from chlorobenzene (CB) or chloroform solution (from ~ 1% wt to ~ 2% wt .) of DPP-PDI block copolymer. The top electrode consists of a 1 nm thick layer of lithium fluoride (LiF) followed by a 60 nm thick layer of aluminum (Al) deposited by thermal evaporation under ~ 2x10^{-6} mbar vacuum. Layer thicknesses were measured by Ambios Tech XP-1 High Reslution profilometer. The active area of each cell was 6 mm^2. Thermal annealing was done by directly placing the completed devices on a digitally controlled hot plate at various temperatures, inside the glove box filled with nitrogen gas. After annealing, the devices were placed on a metal plate and cooled to room temperature prior to conducting measurements. All current voltage (J-V) characteristics of the devices were measured using a Keithley 2400 source meter under AM 1.5G-filtered irradiation (100 mW cm^{-2}) from a 1 kW Oriel solar simulator. The light intensity was measured with an Oriel radiant power meter.

Acknowledgements

This work was supported by the Energy Fronier Research Center on Polymer-based materials for Harvesting Solar Energy through the Department of Energy Office of Basic Energy Sciences under contract DE-SC0001087. Prof.S. Koyuncu gratefully acknowledges the support from Scientific and Technical Research Council of Turkey (TUBITAK) for 2219-International Postdoctoral Research Scholarship Program.

[a]Department of Chemical Engineering, Faculty of Engineering, Canakkale Onsekiz Mart University, 17020, Canakkale (Turkey), e-mail: skoyuncu@comu.edu.tr
[b]Department of Polymer Science and Engineering, University of Massachusetts Amherst, 120 Governors Drive, Amherst, MA 01003 (USA), e-mail: russell@mail.pse.umass.edu

†Electronic Supplementary Information (ESI) available: See DOI: 10.1039/b000000x/

References

1. H. Shirakawa, E. J. Louis, A. G. Macdiarmid, C. K. Chiang and A. J. Heeger, *J Chem Soc Chem Comm*, 1977, 578-580.
2. Y. Cao, P. Smith and A. J. Heeger, *Synthetic Met*, 1992, **48**, 91-97.
3. A. J. Heeger, *Angew Chem Int Edit*, 2001, **40**, 2591-2611.
4. K. M. Coakley and M. D. McGehee, *Chem Mater*, 2004, **16**, 4533-4542.
5. C. J. Brabec, N. S. Sariciftci and J. C. Hummelen, *Adv Funct Mater*, 2001, **11**, 15-26.
6. S. E. Shaheen, C. J. Brabec, N. S. Sariciftci, F. Padinger, T. Fromherz and J. C. Hummelen, *Appl Phys Lett*, 2001, **78**, 841-843.
7. F. Hide, M. A. DiazGarcia, B. J. Schwartz and A. J. Heeger, *Accounts Chem Res*, 1997, **30**, 430-436.
8. A. O. Patil, Y. Ikenoue, F. Wudl and A. J. Heeger, *J Am Chem Soc*, 1987, **109**, 1858-1859.
9. C. Y. Yang, Y. Cao, P. Smith and A. J. Heeger, *Synthetic Met*, 1993, **53**, 293-301.
10. I. Botiz and S. B. Darling, *Macromolecules*, 2009, **42**, 8211-8217.
11. M. Q. Wang, Y. Q. Lian and X. G. Wang, *Curr Appl Phys*, 2009, **9**, 189-194.
12. M. W. Matsen and F. S. Bates, *J Chem Phys*, 1997, **106**, 2436-2448.
13. S. M. Lindner and M. Thelakkat, *Macromol Chem Physic*, 2006, **207**, 2084-2092.
14. M. Sommer, A. S. Lang and M. Thelakkat, *Angew Chem Int Edit*, 2008, **47**, 7901-7904.
15. Q. L. Zhang, A. Cirpan, T. P. Russell and T. Emrick, *Macromolecules*, 2009, **42**, 1079-1082.
16. J. U. Lee, A. Cirpan, T. Emrick, T. P. Russell and W. H. Jo, *J Mater Chem*, 2009, **19**, 1483-1489.
17. J. Roncali, *Macromol Rapid Comm*, 2007, **28**, 1761-1775.
18. F. Wudl, M. Kobayashi, N. Colaneri, M. Boysel and A. J. Heeger, *Mol Cryst Liq Cryst*, 1985, **118**, 199-204.

19. F. Meyers, A. J. Heeger and J. L. Bredas, *Synthetic Met*, 1993, **57**, 4308-4313.
20. F. Meyers, A. J. Heeger and J. L. Bredas, *J Chem Phys*, 1992, **97**, 2750-2758.
21. E. Bundgaard and F. C. Krebs, *Sol Energ Mat Sol C*, 2007, **91**, 954-985.
22. R. S. Kularatne, H. D. Magurudeniya, P. Sista, M. C. Biewer and M. C. Stefan, *J Polym Sci Pol Chem*, 2013, **51**, 743-768.
23. J. M. Jiang, M. C. Yuan, K. Dinakaran, A. Hariharan and K. H. Wei, *J Mater Chem A*, 2013, **1**, 4415-4422.
24. W. Y. Nie, C. M. MacNeill, Y. Li, R. E. Noftle, D. L. Carroll and R. C. Coffin, *Macromol Rapid Comm*, 2011, **32**, 1163-1168.
25. Y. M. Sun, G. C. Welch, W. L. Leong, C. J. Takacs, G. C. Bazan and A. J. Heeger, *Nat Mater*, 2012, **11**, 44-48.
26. H. Y. Chen, J. H. Hou, S. Q. Zhang, Y. Y. Liang, G. W. Yang, Y. Yang, L. P. Yu, Y. Wu and G. Li, *Nat Photonics*, 2009, **3**, 649-653.
27. Y. Y. Liang, Z. Xu, J. B. Xia, S. T. Tsai, Y. Wu, G. Li, C. Ray and L. P. Yu, *Adv Mater*, 2010, **22**, E135-+.
28. S. C. Price, A. C. Stuart, L. Q. Yang, H. X. Zhou and W. You, *J Am Chem Soc*, 2011, **133**, 4625-4631.
29. H. X. Zhou, L. Q. Yang, A. C. Stuart, S. C. Price, S. B. Liu and W. You, *Angew Chem Int Edit*, 2011, **50**, 2995-2998.
30. C. E. Small, S. Chen, J. Subbiah, C. M. Amb, S. W. Tsang, T. H. Lai, J. R. Reynolds and F. So, *Nat Photonics*, 2012, **6**, 115-120.
31. N. Horiuchi and S. Wenham, *Nat Photonics*, 2012, **6**, 136-137.
32. Z. C. He, C. M. Zhong, S. J. Su, M. Xu, H. B. Wu and Y. Cao, *Nat Photonics*, 2012, **6**, 591-595.
33. J. Roncali, *Adv Energy Mater*, 2011, **1**, 147-160.
34. L. J. Bu, X. Y. Guo, B. Yu, Y. Qu, Z. Y. Xie, D. H. Yan, Y. H. Geng and F. S. Wang, *J Am Chem Soc*, 2009, **131**, 13242-+.
35. C. Guo, Y.-H. Lin, M. D. Witman, A. S. Kendall, C. Wang, A. Hexemer, J. Strazalka, E. D. Gomez and R. Verduzco, *Nano Letters*, 2013, **13**, 2957.
36. S. Koyuncu, C. Zafer, F. B. Koyuncu, B. Aydin, M. Can, E. Sefer, E. Ozdemir and S. Icli, *J Polym Sci Pol Chem*, 2009, 47, 6280-6291.
37. S. Y. Qu and H. Tian, Chem Commun, 2012, 48, 3039-3051.
38. G. Yu, Y. Yang, Y. Cao, Q. Pei, C. Zhang and A. J. Heeger, Chemical Physics Letters, 1996, 259, 465-468.

